Bull Math Biol (2014) 76:799–818
DOI 10.1007/s11538-013-9844-3

Society for Mathematical Biology

ORIGINAL ARTICLE

Multiscale Stochastic Reaction–Diffusion Modeling: Application to Actin Dynamics in Filopodia

Radek Erban · Mark B. Flegg · Garegin A. Papoian

Received: 4 December 2012 / Accepted: 12 April 2013 / Published online: 3 May 2013

Abstract Two multiscale (hybrid) stochastic reaction–diffusion models of actin dynamics in a filopodium are investigated. Both hybrid algorithms combine compartment-based and molecular-based stochastic reaction–diffusion models. The first hybrid model is based on the models previously developed in the literature. The second hybrid model is based on the application of a recently developed two-regime method (TRM) to a fully molecular-based model, which is also developed in this paper. The results of hybrid models are compared with the results of the molecular-based model. It is shown that both approaches give comparable results, although the TRM model better agrees quantitatively with the molecular-based model.

1 Introduction

In recent years, several stochastic reaction–diffusion algorithms have been introduced for modeling in cellular and molecular biology, including Smoldyn (Andrews and Bray 2004), SpatioCyte (Arjunan and Tomita 2010), URDME (Engblom et al. 2009), MesoRD (Hattne et al. 2005), STEPS (Hepburn et al. 2012), first-passage kinetic Monte Carlo method (Opplestrup et al. 2009), MCell (Stiles and Bartol 2001), and Green's function reaction dynamics (van Zon and ten Wolde 2005). Some of these methods simulate trajectories and reactive collisions of individual

R. Erban (✉) · M.B. Flegg
Mathematical Institute, University of Oxford, 24-29 St. Giles', Oxford OX1 3LB, UK
e-mail: erban@maths.ox.ac.uk

M.B. Flegg
e-mail: flegg@maths.ox.ac.uk

G.A. Papoian
Department of Chemistry & Biochemistry, University of Maryland, Chemistry Bldg 2216, College Park, MD 20742-2021, USA
e-mail: gpapoian@umd.edu

biomolecules (Andrews and Bray 2004; van Zon and ten Wolde 2005). Other approaches divide the computational domain into compartments and simulate the time evolution of the numbers of molecules in these compartments (Engblom et al. 2009; Hattne et al. 2005). Some models explicitly model intracellular crowding and excluded volume effects (Arjunan and Tomita 2010), while other algorithms describe biomolecules as point-like particles (Andrews and Bray 2004). High-resolution (detailed, molecular-based) models are often more computationally intensive than compartment-based (coarser) models. However, a higher level of detail is sometimes only needed in a relatively small part of the computational domain. Then there is a potential to speed up simulations by developing hybrid approaches, which can efficiently and accurately use models with a different level of detail in different parts of the computational domain (Flegg et al. 2012; Franz et al. 2013).

The development of successful hybrid models requires understanding of connections between detailed and coarser models of stochastic reaction–diffusion processes (Erban and Chapman 2007, 2009). The optimal choice of a stochastic reaction–diffusion algorithm also depends on the particular biological problem, which is modeled. In this paper, our main application area is modeling of actin dynamics in filopodia (Lan and Papoian 2008), although very similar issues also arise in modeling of three-dimensional actin networks in lamellipodia (Hu and Papoian 2010). In this area, previously developed models have been formulated as a combination of molecular-based and compartment-based (coarser) approaches (Lan and Papoian 2008; Zhuravlev and Papoian 2009; Hu and Papoian 2010; Zhuravlev et al. 2012). These and related developments in filopodia modeling were recently reviewed in Zhuravlev and Papoian (2011). In the current work, we will compare the corresponding (less-detailed) hybrid modeling approaches with a fully molecular-based (detailed) model developed here. On the face of it, a more accurate description of biology can be obtained by introducing additional details into the model, but this could also include significant challenges, for example, (i) an increase in the computational intensity of the algorithm; and (ii) an increase in the number of unknown parameters. In this paper, we will study which molecular-based details can be replaced by coarser compartment-based methods (without a significant loss in accuracy), and which molecular-based components of the model are essential and require a description with higher resolution.

The paper is organized as follows. In Sect. 2, we summarize the modeling of actin dynamics in filopodia. We discuss stochastic reaction–diffusion models in the literature and a simplified hybrid model, which is used in the paper as an illustrative example. In Sect. 3, we introduce a fully molecular-based model and the connections between the presented models are analyzed. We show that the simplified hybrid model underestimates the average filament length by 5 % when compared with the fully molecular-based model. In Sect. 4, we present a different approach to hybrid simulations of actin dynamics based on the recently developed two-regime method (TRM) (Flegg et al. 2012). We show that the results computed by the TRM compare well with the fully molecular-based model. Moreover, the TRM can save the computational time by using a less-detailed (compartment-based) model in a part of the computational domain. The TRM in Sect. 4 makes use of a time-dependent interface between compartment-based and molecular-based parts of the simulation. This is a

generalization of the previously published TRM (Flegg et al. 2012), which has been developed for a fixed interface between different regimes. We conclude this paper with the discussion in Sect. 5.

2 Actin Dynamics in Filopodia: A Paradigm for Multiscale Stochastic Reaction–Diffusion Modeling

Filopodium is an elongated organelle, which grows out of the cell to probe the environment for mechanical obstacles or chemical cues (Zhuravlev and Papoian 2011). It is used by a number of motile cells including metastatic cancer cell (Yamazaki et al. 2005) or the wound healing cells (Noselli 2002). Filopodium is composed from a set of parallel actin filaments bundled together and rooted in the lamellipodium (Zhuravlev and Papoian 2011; Schaus et al. 2007). In Fig. 1(a), we present a schematic model of actin dynamics in a filopodium, which is used in Zhuravlev and Papoian (2009). This model uses both compartment-based and molecular-based approaches to reaction–diffusion modeling. The key components of this model are the following three processes:

[P1] compartment-based description of diffusion of G-actin molecules;
[P2] off-lattice modeling of growth of F-actin filaments; and
[P3] retrograde flow which pulls back F-actin filaments.

In addition to [P1]–[P3], Fig. 1(a) includes capping proteins which are explicitly modeled in Zhuravlev and Papoian (2009), but we will not consider their effects in this paper. In this section, we will study a minimal model which includes [P1]–[P3]. This model is schematically shown in Fig. 1(b). We will show that it can capture essential features of filopodial dynamics. We will compare it with the fully molecular-based model in Sect. 3.

2.1 Minimal Hybrid Model of Actin Dynamics in Filopodia

Our minimal hybrid model of actin dynamics is a simplified version of the hybrid model presented in Zhuravlev and Papoian (2009). Considering processes [P1]–[P3], the minimal model describes the dynamics of G-actin (the monomer form of actin) and F-actin (the polymer form of actin) in a filopodium.

Following Zhuravlev and Papoian (2009), we will divide the growing filopodium into $N \equiv N(t)$ compartments (cylinders) of height h (see Fig. 1(b)). Here, h is a constant during simulations and $N(t)$ is a positive integer. Therefore, we implicitly assume that the filopodium has the height equal to the integer multiple of h. The filopodium grows in a discrete way, by adding and removing a full compartment whenever necessary. The number of G-actin molecules in the jth compartment will be denoted as $A_j \equiv A_j(t)$, $j = 1, 2, \ldots, N(t)$. Here, the first compartment is next to the cell interior, a bulk source of G-actin. Another variable of the model is the averaged position of "the barbed ends" of actin filaments (F-actin). It is denoted as $X \equiv X(t)$ (red dot in Fig. 1(b)). It is postulated that the barbed ends are always in the last compartment, i.e. $X(t) \in [(N(t) - 1)h, N(t)h]$.

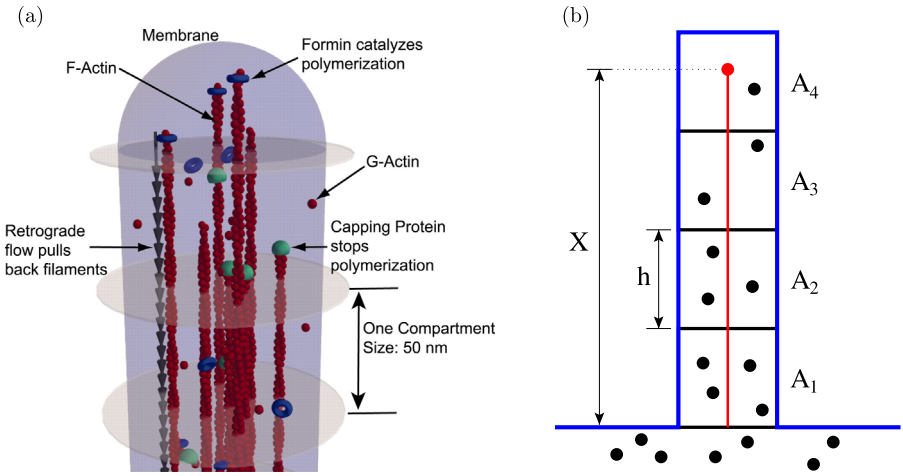

Fig. 1 (**a**) Schematic representation of the actin dynamics model used in Zhuravlev and Papoian (2009). Reprinted with permission from Zhuravlev and Papoian (2009). (**b**) Schematic of the simplified hybrid model for $N(t) = 4$

"Treadmilling" of actin filaments (F-actin) has been previously modeled by an off-lattice model (Zhuravlev and Papoian 2009; Zhuravlev et al. 2010). In our minimal model, we consider a bundle of F-actin filaments in the center of the filopodium (red line in Fig. 1(b)), without differentiating individual filaments within the bundle, i.e., treating the bundle growth in an average way. Polymerization (resp. depolymerization) with the rate k^+ (resp. k^-) is considered at the barbed end of the bundle. G-actin molecules diffuse with the diffusion constant D. Thus, the compartment-based part of the model is subject to the following reactions (Erban et al. 2007; Erban and Chapman 2009):

$$A_N \underset{k^-}{\overset{k^+}{\rightleftarrows}} \emptyset, \tag{1}$$

$$\emptyset \underset{d}{\overset{d\overline{A}}{\rightleftarrows}} A_1 \underset{d}{\overset{d}{\rightleftarrows}} A_2 \underset{d}{\overset{d}{\rightleftarrows}} A_3 \underset{d}{\overset{d}{\rightleftarrows}} \cdots \underset{d}{\overset{d}{\rightleftarrows}} A_N \tag{2}$$

where

$$d = \frac{D}{h^2}.$$

Chemical reactions (1) describe polymerization and depolymerization where $\emptyset$ denotes a source or a sink of the molecules (in the compartment-based part of the model) which correspond to these events. The chain of reactions (2) describes the diffusion of G-actin. Molecules are introduced into the domain with a fixed rate $d\overline{A}$, which corresponds to the constant concentration of G-actin molecules in the cytosol.

The compartment-based part (1)–(2) of the model can be simulated by the Gillespie stochastic simulation algorithm (SSA) (Gillespie 1977), or its variants (Gibson and Bruck 2000; Cao et al. 2004). These are event-based algorithms,

Table 1 Pseudocode of one time step of the minimal hybrid model of actin dynamics in a filopodium

[A1]	Compute the time when the next compartment-based event happens as $t+\tau$, where t is the current time and the time step τ is computed by (3) with the help of a random number r uniformly distributed in $(0, 1)$
[A2]	Use another uniformly distributed random number to compute which compartment-based event (1)–(2) happens at time $t+\tau$
[A3]	If a diffusion jump (2) occurs at time $t+\tau$, then update the numbers of G-actin molecules in the corresponding compartment(s). Put $X(t+\tau) = X(t)$
[A4]	If the polymerization reaction $A_N \xrightarrow{k^+} \emptyset$ in (1) occurs at time $t+\tau$, then $A_N(t+\tau) = A_N(t) - 1$; $X(t+\tau) = X(t) + \delta$ where δ is the constant monomer length
[A5]	If the depolymerization reaction $\emptyset \xrightarrow{k^-} A_N$ in (1) occurs at time $t+\tau$, then $A_N(t+\tau) = A_N(t) + 1$; $X(t+\tau) = X(t) - \delta$
[A6]	Retrograde flow pulls back the F-actin filament with velocity v, i.e., $X(t+\tau) := X(t+\tau) - v\tau$ where $X(t+\tau)$ on the right-hand side was computed in one of the steps [A3]–[A5]
[A7]	If $X(t+\tau)$ is no longer in the last compartment, then update $N(t+\tau)$ using (4) and update numbers of molecules in the last compartment using (5)–(6)
[A8]	Continue with the step [A1] where the current time t is updated to $t+\tau$

which means that they calculate the time of the next event (reaction or diffusive jump) stochastically, rather than evolving the simulation using a predefined fixed time step. The Gillespie SSA makes use of propensity functions (Gillespie 1977; Erban et al. 2007). The total propensity function at time t for the system (1)–(2) can be computed by

$$\alpha_0(t) = k^+ A_N(t) + k^- + d\overline{A} + d A_N(t) + 2d \sum_{i=1}^{N-1} A_i(t)$$

and the time to the next reaction or diffusion event is

$$\tau = \frac{1}{\alpha_0} \log\left(\frac{1}{r}\right), \tag{3}$$

where r is uniformly distributed random number in $(0, 1)$. Once the time to the next event τ is computed using (3), the Gillespie SSA decides which (reaction or diffusion) event occurs using another uniformly distributed random number in $(0, 1)$. For example, the polymerization event happens with the probability $k^+ A_N(t)/\alpha_0$ and the depolymerization with the probability k^-/α_0.

One step of the minimal hybrid algorithm is presented in Table 1 as the algorithm [A1]–[A8]. The compartment-based part (1)–(2) is coupled with the off-lattice part of the model which describes the time evolution of the F-actin filament length $X(t)$. It is evolved using the Gillespie time steps (3). At each time step, three events can happen which change $X(t)$. If the polymerization reaction occurs in the step [A4], then $X(t+\tau) = X(t) + \delta$ where δ is the constant monomer length. If the depolymerization reaction occurs in the step [A5], then $X(t+\tau) = X(t) - \delta$. Finally, retrograde flow pulls back the F-actin filament with velocity v, which is implemented in the step [A6].

Table 2 Parameters of the minimal hybrid model of actin dynamics

Compartment height	$h = 50$ nm
Diffusion of G-actin	$D = 5/16\ \mu\text{m}^2\,\text{s}^{-1}$
Polymerization rate (in the last compartment)	$A_{N(t)}k^+$ where $k^+ = 21.8\ \text{s}^{-1}$
Depolymerization rate	$k^- = 1.4\ \text{s}^{-1}$
Effective monomer size	$\delta = 2.7$ nm
Retrograde flow speed	$v = 70$ nm/s
Bulk concentration of G-actin multiplied by V	$\overline{A} = 5.3$

In the step [A7], we evolve the length of filopodium. We have to make sure that the barbed filament end is in the last compartment, i.e., $X(t) \in [(N(t)-1)h, N(t)h]$. Thus, the number of compartments $N(t)$ is evolved as follows:

$$N(t+\tau) = \left\lceil \frac{X(t+\tau)}{h} \right\rceil, \tag{4}$$

where $X(t+\tau)$ is computed by the steps [A4]–[A6] and $\lceil \cdot \rceil$ is the ceiling function, i.e., $\lceil X(t+\tau)/h \rceil$ is the smallest integer not less than $X(t+\tau)/h$. If the number of compartments $N(t+\tau)$ differs from $N(t)$, then we have to also update the number of G-actin molecules $A_{N(t+\tau)}$, which are in the last compartment. The most natural way is to conserve the number of G-actin molecules in the step [A7]. This leads to the following rules:

$$\text{if } N(t+\tau) = N(t) - 1, \quad \text{then } A_{N(t+\tau)}(t+\tau) := A_{N(t)}(t+\tau) + A_{N(t)-1}(t+\tau), \tag{5}$$

$$\text{if } N(t+\tau) = N(t) + 1, \quad \text{then } A_{N(t+\tau)}(t+\tau) := 0, \tag{6}$$

where $A_{N(t)}(t+\tau)$ and $A_{N(t)-1}(t+\tau)$ on the right-hand side of (5) are numbers computed in the previous steps [A1]–[A6]. If $N(t+\tau) = N(t)$, then the number of molecules in the last compartment does not change and it is not updated in the step [A7].

2.2 Illustrative Computational Results

The minimal hybrid model [A1]–[A8] has seven parameters D, k^+, k^-, h, $\overline{A}$, δ, and v. Their values are based on the previous models (Zhuravlev and Papoian 2009; Zhuravlev et al. 2010) and are summarized in Table 2. To calculate $\overline{A}$, we consider that the bulk concentration of G-actin is 10 μM and that the filopodium diameter is $a = 150$ nm. Then each compartment is a cylinder with volume $V = \pi a^2 h/4$ and the bulk concentration of G-actin corresponds to 5.3 molecules per compartment. The polymerization rate k^+ is the rate per one molecule (in the last compartment of volume V) per unit of time.

In the steps [A5]–[A6], we add or subtract the monomer length δ. The constant δ can be considered as an effective monomer length, rather than the diameter of G-actin, because F-actin consists of two protofilaments in a right-handed helix (Zhuravlev et al. 2010). Therefore, models in the literature choose δ equal to the half actin

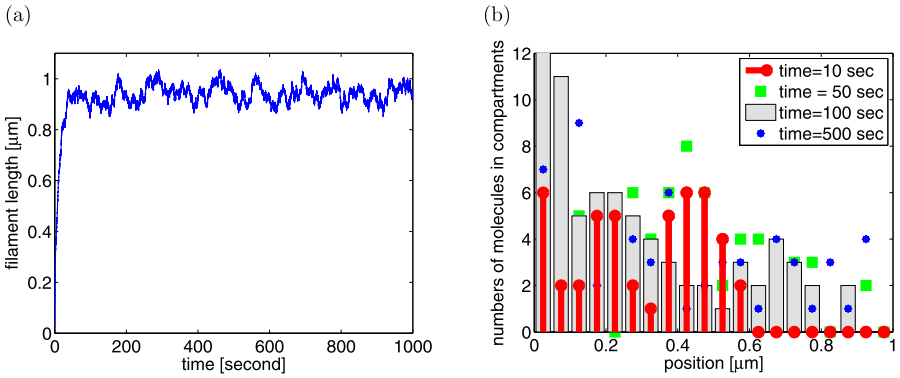

Fig. 2 Results computed by the minimal hybrid model [A1]–[A8] for parameters given in Table 2. (**a**) Time evolution of filament length $X(t)$. (**b**) Snapshots of numbers of molecules in compartments $A_j(t)$, $j = 1, 2, \ldots, N(t)$, at four different times

monomer size 2.7 nm (Zhuravlev and Papoian 2009; Zhuravlev et al. 2010). Since there are typically 10–30 filaments per filopodium, the half actin monomer size can be further divided by the estimated number of filaments in the filopodium to calculate the effective monomer length δ. In our case, we will use $\delta = 2.7$ nm and we will rescale the diffusion constant by the factor of 16. Then our minimal hybrid model (with one filament) will lead to similar filopodium stationary lengths as the models in the literature which consider several filaments (Zhuravlev and Papoian 2009; Zhuravlev et al. 2010).

In Fig. 2(a), we present the time evolution of the filament length $X(t)$. In Fig. 2(b), we plot numbers of molecules in each compartment $A_1, A_2, \ldots, A_{N(t)}$ at four different times. Comparing panels (a) and (b) of Fig. 2, we observe that the snapshot of $A_1, A_2, \ldots, A_{N(t)}$ at time 10 seconds only includes compartments up to position 0.6 μm, because the filament length have not yet reached its equilibrium values. The filopodium reaches a steady state length (approximately 1 μm) because the transport flux of G-actin monomers continuously diminishes as the tube becomes longer. Hence, at a certain steady state length, L_s, the polymerization flux of actin monomers at the tip equals the removal of actin from the tube via the retrograde flow process. A simple mean-field expression for the steady-state length of filopodia was derived in Lan and Papoian (2008) and further elaborated in Zhuravlev and Papoian (2011). Using our notation, the mean-field approximation of the stationary filopodium length can be written as follows (Zhuravlev and Papoian 2011)

$$L_s = \frac{D\delta}{vh}\left(\overline{A} - \frac{k^-}{k^+}\right) - \frac{D}{hk^+}. \tag{7}$$

Using the parameter values given in Table 2, we obtain $L_s = 0.98$ μm. We can also see that $k^-/k^+ \doteq 6.4 \times 10^{-2}$ is much smaller than $\overline{A} = 5.3$. In particular, the mean-field estimate (7) is not significantly influenced by depolymerization.

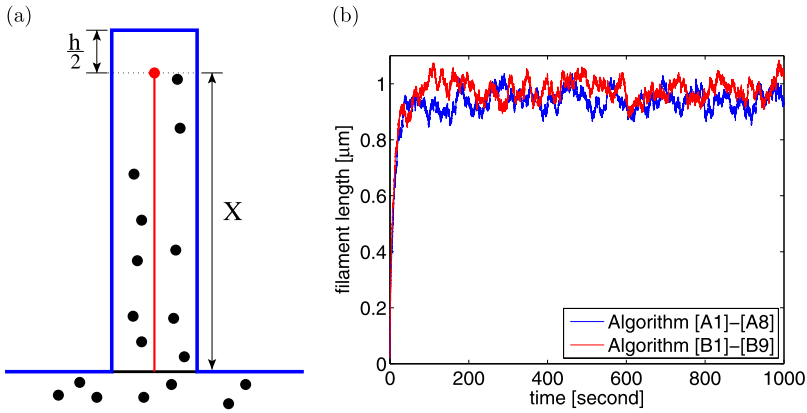

Fig. 3 (**a**) Schematic representation of the simplified molecular-based (off-lattice) model. (**b**) Time evolution of the filament length $X(t)$ computed by the minimal hybrid model [A1]–[A8] (*blue line*) and the molecular-based model [B1]–[B9] (*red line*). Parameters are given in Table 2

3 Molecular-Based Modeling of Actin Dynamics

In this section, we introduce a molecular-based model which does not include any compartments. It is schematically shown in Fig. 3(a). The position of every G-actin molecule is modeled explicitly. At time t, we have $n(t)$ G-actin molecules in the filopodium at positions $y_i(t)$, $i = 1, 2, \ldots, n(t)$. We choose a fixed time step Δt and evolve $y_i(t)$ according to the discretized Brownian motion (Erban et al. 2007):

$$y_i(t + \Delta t) = y_i(t) + \sqrt{2D\Delta t}\xi_i, \tag{8}$$

where ξ_i are normally distributed random numbers with zero mean and unit variance. The evolution equation (8) replaces (2). In our simulations, we will use the time step $\Delta t = 10^{-6}$ s. In particular, the average step size during one time step $\sqrt{2D\Delta t}$ (i.e., the square root of the mean squared displacement) is equal to 0.79 nm for parameter values given in Table 2. This is much smaller than the compartment size $h = 50$ nm of the minimal hybrid model, which was introduced in Sect. 2.1.

In order to have a fair comparison with the minimal hybrid model, we will postulate that the filopodium end is at a fixed distance $h/2$ above the barbed end of the F-actin filament. Therefore,

$$y_i(t) \in \left[0, X(t) + \frac{h}{2}\right], \quad \text{for } i = 1, 2, \ldots, n(t). \tag{9}$$

One time step of the molecular-based algorithm is presented in Table 3 as the algorithm [B1]–[B9]. The boundary conditions for the off-lattice model (8) are implemented in steps [B2]–[B5]. We use the same boundary conditions as for the compartment-based model (2). We implement a reflective boundary condition at $X(t)+h/2$ in the step [B2]. Conditions [B3]–[B4] implement the adsorbing boundary condition at the bulk end $\{y = 0\}$, which corresponds to the diffusive jump $A_1 \to \emptyset$ in (2). Obviously, if $y_i(t + \Delta t)$ computed by (8) is negative, then the molecule has to be removed from the system (step [B3]). However, there is a chance that a molecule

Table 3 Pseudocode of one time step of the molecular-based model of actin dynamics in a filopodium

[B1]	Put $n(t+\Delta t)=n(t)$. Compute the positions of all molecules $y_i(t+\Delta t)$, $i=1,2,\ldots,n(t+\Delta t)$, at time $t+\Delta t$ using (8)
[B2]	If $y_i(t+\Delta t)$, $i=1,2,\ldots,n(t+\Delta t)$, computed by (8) is greater than $X(t)+h/2$, then $y_i(t+\Delta t)=2X(t)+h-y_i(t)-\sqrt{2D\Delta t}\xi_i$ (mirror reflection)
[B3]	If $y_i(t+\Delta t)$, $i=1,2,\ldots,n(t+\Delta t)$, computed by (8) is negative, then remove the ith molecule from the system
[B4]	If $y_i(t+\Delta t)$, $i=1,2,\ldots,n(t+\Delta t)$, computed by (8) is positive, then remove the ith molecule from the system with probability $\exp[-y_i(t)y_i(t+\Delta t)/(D\Delta t)]$
[B5]	Introduce a new G-actin molecule to the system with probability given by (10). Its initial position $y_j(t+\Delta t)$ is a random number sampled from the distribution (11). Here, the value of $n(t+\Delta t)$ is increased by one and $j=n(t+\Delta t)$
[B6]	Put $X(t+\Delta t)=X(t)$. G-actin molecules satisfying $y_i(t+\Delta t)\in[X(t)-h/2, X(t)+h/2]$ bind to the barbed end with probability $k^+\Delta t$. If this happens, then the corresponding molecule is removed from the solution and $X(t+\Delta t)$ is updated by adding δ
[B7]	Depolymerization occurs with probability $k^-\Delta t$. It this happens, then $n(t+\Delta t)$ is increased by one, a new G-actin molecule is introduced at $y_j(t+\Delta t)=X(t+\Delta t)$ where $j=n(t+\Delta t)$, and $X(t+\Delta t)$ is updated by subtracting the monomer length δ
[B8]	Update $X(t+\Delta t)$ by subtracting $v\Delta t$ (retrograde flow)
[B9]	Continue with the step [B1] where the current time t is updated to $t+\Delta t$

hit the boundary during the finite time step even if $y_i(t+\Delta t)$ computed by (8) is positive; that is, during the time interval $[t, t+\Delta t]$ the molecule might have crossed to y_i negative and then crossed back to y_i positive again (Andrews and Bray 2004; Erban and Chapman 2007). This case is implemented in the step [B4]. The introduction of molecules from the bulk (which corresponds to the diffusive jump $\emptyset \to A_1$ in (2)) is simulated in the step [B5]. We introduce a new G-actin molecule to the system with the probability

$$\frac{2\overline{A}}{h}\sqrt{\frac{D\Delta t}{\pi}} \tag{10}$$

during each time step. If the molecule is introduced to the domain, then it is initialized at a randomly chosen position x distributed according to the probability distribution

$$\sqrt{\frac{\pi}{4D\Delta t}}\operatorname{erfc}\left(\frac{x}{\sqrt{4D\Delta t}}\right) \tag{11}$$

where $\operatorname{erfc}(z)=2/\sqrt{\pi}\int_z^\infty \exp(-s^2)\,\mathrm{d}s$ is the complementary error function. We will see in Sect. 4 that Eqs. (10)–(11) correctly implement the diffusive jump $\emptyset \to A_1$ in (2). They can be considered as a special case of the two-regime method (Flegg et al. 2012). We assume that Δt is chosen small enough, so that (10) is significantly smaller than 1 and can be interpreted as a probability.

The movement of the barbed end of the F-actin filament is governed by polymerization/depolymerization of G-actin and retrograde flow in an identical way to that in Sect. 2.1. It is given in the steps [B6]–[B8] in Table 3. To simulate the polymerization reaction in the step [B6], all G-actin molecules in the interval $[X(t)-h/2, X(t)+h/2]$ are considered. Each of these molecules can bind to the

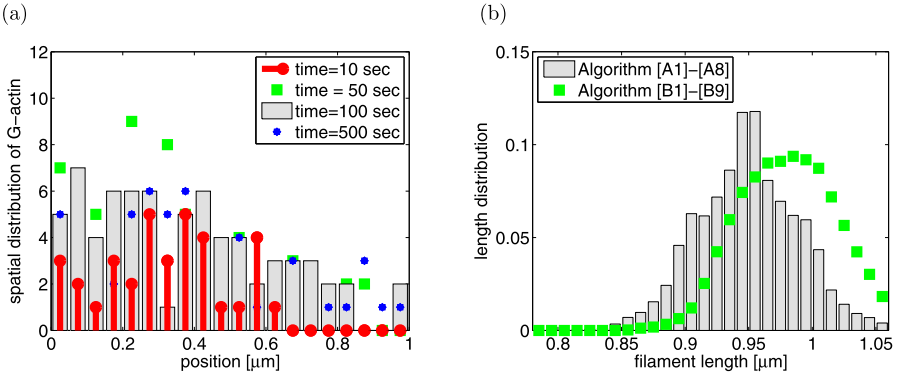

Fig. 4 (**a**) Snapshots of spatial distribution of G-actin at four different times computed by the molecular-based model [B1]–[B9] for the parameters given in Table 2 and $\Delta t = 10^{-6}$ s. (**b**) The stationary distribution of the filament length X for the parameters given in Table 2 computed by algorithms [A1]–[A8] (*gray histogram*) and [B1]–[B9] (*green squares*)

barbed end with probability $k^+\Delta t$ (provided that Δt is chosen small enough). Depolymerization occurs with probability $k^-\Delta t$ in the step [B7]. In this case, a new G-actin molecule is introduced at $X(t+\Delta t)$ and $X(t+\Delta t)$ is updated by subtracting the monomer length. This method of polymerization and depolymerization is specifically chosen to imitate the reaction kinetics that are implemented in the hybrid method in Sect. 2.1. If a new G-actin molecule is added (resp. removed) from the system, we have to update the total number of simulated molecules $n(t+\Delta t)$ accordingly.

3.1 Illustrative Computational Results

We use the parameters from Table 2 and the time step $\Delta t = 10^{-6}$ s. In particular, the probabilities $k^+\Delta t \doteq 2.18 \times 10^{-5}$ and $k^-\Delta t \doteq 1.4 \times 10^{-6}$ are much smaller than 1 and the steps [B6]–[B7] correctly implement the polymerization and depolymerization events. The value of (10) is 6.69×10^{-2} and can also be interpreted as a probability.

The time evolution of the filament length $X(t)$ is presented in Fig. 3(b). We compare it with the result of the minimal hybrid model [A1]–[A8] (introduced in Sect. 2.1). Snapshots of spatial distribution of G-actin molecules are presented in Fig. 4(a). We visualize numbers of molecules in cylinders of the height h. Therefore, Fig. 4(a) can be directly compared with Fig. 2(b). The stationary distribution of filament lengths obtained from a long time simulation of the molecular based model [B1]–[B9] is presented in Fig. 4(b). It was obtained by binning the time series of the length 10^4 seconds. We compare the resulting distribution (green squares) with the stationary distribution computed by the minimal hybrid model [A1]–[A8]. Since the minimal hybrid model [A1]–[A8] is less computationally intensive, we can easily compute longer time series. In Fig. 4(b), we present the stationary distribution estimated from the time series of the length 10^5 seconds (gray histogram). We see that the distribution computed by the molecular-based model [B1]–[B9] is shifted to

the right of the distribution computed by the minimal hybrid model [A1]–[A8] by approximately 5 %.

3.2 Connections Between Models [A1]–[A8] and [B1]–[B9]

In Figs. 2, 3, and 4, we observe that both models [A1]–[A8] and [B1]–[B9] give comparable results. However, we also see that there is a quantitative difference between the results computed by these two models in Fig. 4(b). In this section, we will discuss what is the reason for this quantitative difference. In Sect. 4, we will design a different hybrid model which better agrees with the molecular-based algorithm [B1]–[B9].

It is relatively straightforward to estimate the expected steady state filament length L_s at the mean-field level (Zhuravlev and Papoian 2011). Let $c(x)$ be the steady-state concentration of G-actin measured in the number of molecules per unit of volume. Considering the domain definition (9) of the algorithm [B1]–[B9], the steady-state concentration $c(x)$ is defined for $x \in [0, L_s + h/2]$. The bulk concentration is constant and equal to $c(0) = \overline{A}/V$ where $\overline{A}$ is given in Table 2, $V = \pi a^2 h/4$ and a is the filopodium diameter (we use $a = 150$ nm in our simulations). The steady-state concentration $c(x)$ is linear in the region between the bulk $x = 0$ and the filament tip $x = L_s$, i.e.,

$$c(x) = \frac{\overline{A}}{V} - \beta x, \quad \text{for } x \in [0, L_s] \tag{12}$$

where β is a positive constant. At the steady state, the speed of the filament extension (due to polymerization) is balanced by the depolymerization and the retrograde flow, i.e.,

$$k^+ V c(L_s)\delta = k^- \delta + v. \tag{13}$$

The diffusive flux of G-actin at the filament tip also balances with the difference in polymerization and depolymerization rates. That is,

$$-D\frac{\partial c}{\partial x}(L_s) = \frac{k^+ V c(L_s) - k^-}{V/h}.$$

Using (12) on the left-hand side and (13) on the right-hand side, we obtain

$$\beta = \frac{vh}{DV\delta}.$$

Substituting for β in (12) and evaluating the resulting function at $x = L_s$, we get

$$c(L_s) = \frac{\overline{A}}{V} - \frac{vh}{DV\delta}L_s.$$

Substituting for $c(L_s)$ into (13) and solving for L_s, we obtain the mean field approximation (7). It is worth noting that we have $L_s = 0.976$ μm for our parameter values. In Fig. 4(b), we see that this estimate is closer to the results of the molecular-based model [B1]–[B9] than to the results of the minimal hybrid model [A1]–[A8]. The main reason for the model difference is the additional bias which the minimal hybrid model [A1]–[A8] introduces to modeling. It can be explained as follows.

The motion of the filament tip according to the algorithm [A1]–[A8] depends on the concentration in the last compartment. The mean-field approximation of the expected velocity of the filament tip is given by

$$\frac{d\langle X\rangle}{dt}(t) = -v - k^{-}\delta + \langle A_{N(t)}\rangle k^{+}\delta,$$

where $\langle A_{N(t)}\rangle$ is the average number of G-actin molecules in the last compartment. This distribution can be considered to be a step function approximation of continuous concentration of molecules $c(x,t)$. Assuming that there is minimal error in the expected value of G-actin at the center of compartments, the expected velocity $d\langle X\rangle/dt$ will be overestimated if $X(t) \in (N(t)h - h/2, N(t)h]$ and underestimated if $X(t) \in [(N(t)-1)h, N(t)h - h/2)$. This is because the expected distribution $c(x,t)$ of G-actin monotonically decreases from the bulk to the filopodia tip. The most prominent result of this compartment internal bias of the filament tip is the appearance of local maxima in the likelihood to find the tip at steady state at the compartment edges. The filament tip experiences a bias toward the compartment edges. This can be seen clearly in Fig. 4(b) at 0.9 μm, 0.95 μm, and 1 μm.

The secondary effect that the compartments have on the distribution of the filament tip at steady state is to create a net bias of the tip in the direction of the filopodia base. A filament tip at $X(t) \in (N(t)h - \varepsilon, N(t)h]$ (for small $\varepsilon > 0$) may cross the boundary and create a new compartment according to the step [A7]. Since the new compartment represents the expansion of the filopodia, the G-actin copy number initialized in this new compartment is zero in (6). This sudden void of G-actin molecules , which the filament tip senses is filled at a rate describing the net flux of molecules from one compartment to another compartment. Then the filament tip is more likely to migrate back into its previous compartment due to retrograde flow. This bias results in the likelihood of the filament tip to linger, overall, in compartments closer to the bulk for longer periods than would be expected. In the simulations in this paper, this effect results in the expected filament tip being 5 % shorter in the hybrid model [A1]–[A8] than in the molecular-based model [B1]–[B9]. The effect of this bias would be reduced if the time taken for the new compartment to acquire the correct copy number of G-actin molecules is reduced. This, in principle, could be achieved by reducing the compartment length h. However, this would increase the computational intensity of the algorithm. Moreover, there is also a limit to how small the compartments may be made before the correct polymerization rates could not be simulated (Erban and Chapman 2009). This means that there is a fundamental limit to how accurately this compartment hybrid approach may describe the process that is being modeled.

Algorithm [B1]–[B9] does not have any of the aforementioned artefacts that are implicit with the minimal hybrid model [A1]–[A8]. This is because the distribution of G-actin is described with a continuous distribution and the rate of polymerization is always given as though it were at the center of a compartment (and, therefore, not experiencing compartment edge effects). The disadvantage of the molecular-based model [B1]–[B9] is the computational effort involved in tracking G-actin molecules through the entire domain for the sole purpose of knowing where the G-actin molecule is when it is close to the filament tip. In the next section, we present a different hybrid model which is based on the recently developed two-regime method (Flegg et al. 2012). It uses a compartment-based regime (similar to the algorithm

[A1]–[A8]) away from the filament tip to save time tracking G-actin molecules. This compartment-based region is coupled to a molecular-based regime close to the tip (as it is used in the algorithm [B1]–[B9]).

4 Two-Regime Method Simulations

The modeling approaches [A1]–[A8] and [B1]–[B9] have advantages and disadvantages. On the one hand, the minimal hybrid model [A1]–[A8] is simple and quick to implement. On the other hand, it does not capture in the most accurate way the phenomena that are being modeled. The off-lattice, microscopic model [B1]–[B9] described in Sect. 3 allows for a more precise measurement at the cost of computing trajectories of all G-actin molecules. In this section, we will introduce a different hybrid model, which has the accuracy of the molecular-based model [B1]–[B9]. It will be based on the two-regime method (TRM) which uses a compartment-based approach in regions requiring less detail and a molecular-based approach in regions where accuracy is crucial to the model (Flegg et al. 2012). The modeler chooses a region of interest Ω_M within computational domain Ω to be modeled with an off-lattice microscopic model and separates this part of the domain from the rest of the domain with an interface I. The remaining parts Ω_C of the computational domain are then discretized into compartments (like that observed in Sect. 2.1). Each region is modeled individually as described by the corresponding model. That is, molecules in Ω_C jump according to (2) between compartments and molecules inside Ω_M change position each time step Δt according to (8). Correct coupling of the molecules migrating over the interface I is crucial to ensure that the correct flux of molecules is modeled between Ω_M and Ω_C. In particular, molecules migrate from a compartment that lies on the interface with the propensity

$$\Phi = \frac{2A_{N_C}}{h}\sqrt{\frac{D}{\pi\,\Delta t}}, \tag{14}$$

where A_{N_C} is the number of molecules in the last compartment. They are placed into the microscopic region Ω_M a distance of x (from the interface) generated from a distribution (11). If Δt is sufficiently small, then $\Phi\,\Delta t \ll 1$ can be interpreted as a probability of moving one molecule from Ω_C to Ω_M during one time step Δt (in particular, the TRM can also be used to justify Eq. (10) in Sect. 3). All molecules that are incident on the interface from Ω_M necessary lose their position and become part of the compartment in Ω_C on the other side of the interface.

Filament growth occurs, in our model, at the filament tip. It is apparent that a compartment-based representation of free G-actin at the filament tip is inappropriate to model the reaction at high precision. Modeling the filament growth with a molecular-based model which more accurately simulates the local concentration of molecules was shown to produce quantitatively different results in Fig. 4(b). This, however, comes at the cost of simulating trajectories for each molecule regardless of how close it is to the tip. In this section, we shall use the TRM to simulate the diffusion of molecules away from the tip using a compartment-based approach but a microscopic, off-lattice approach in a region around the tip. The geometry of our TRM model is schematically shown in Fig. 5(a). Following (9), we choose

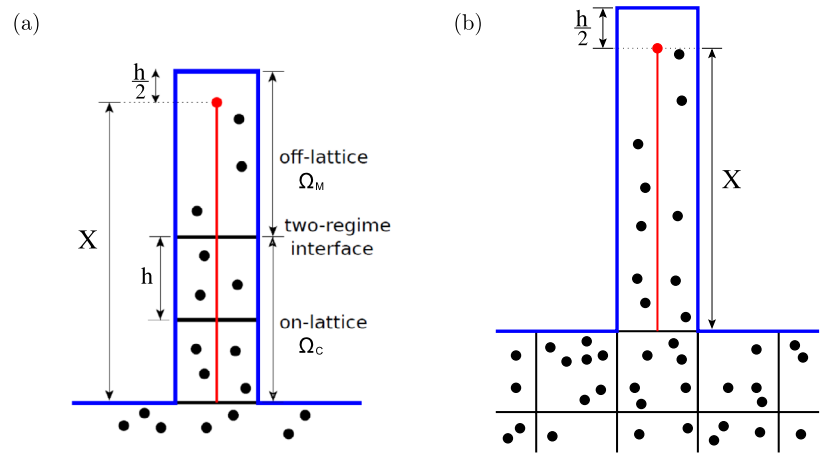

Fig. 5 (**a**) Schematic of the geometry of the TRM simulation, which is used in this manuscript. (**b**) Schematic of an alternative TRM geometry which would be useful for modeling of coupling of the filopodium with the cytosol

$$\Omega = \left[0, X(t) + \frac{h}{2}\right], \qquad \Omega_M(t) = \left[I(t), X(t) + \frac{h}{2}\right], \qquad \Omega_C(t) = \left[0, I(t)\right], \tag{15}$$

where $I(t)$ is the position of the TRM interface at time t, $I = \partial\Omega_M \cap \partial\Omega_C$ and $\Omega = \Omega_M \cup \Omega_C$. In particular, the presented hybrid model is the extension of the TRM approach presented in Flegg et al. (2012) to a scenario, which includes a time dependent interface $I(t)$. We will consider that $I(t)$ can only have discrete values

$$I(t) = N_C(t)h, \tag{16}$$

where $N_C(t)$ is the number of compartments in Ω_C and h is the compartment length. One iteration of the TRM algorithm is presented in Table 4 as the algorithm [C1]–[C8]. Since the compartment-based part of the model is simulated by an event-based algorithm, the current time in Ω_C is no longer a multiple of Δt. We will denote it as t_C. It is updated using (3) in the step [C1]. Molecular-based events in Ω_M are still updated at multiples of Δt. We will keep track of them using the time variable

$$t_M \in \{0, \Delta t, 2\Delta t, 3\Delta t, \ldots\}, \tag{17}$$

which is the time when the last update of variables corresponding to the molecular-based regime Ω_M took place.

Initially, the model is identical to the molecular-based model in Sect. 3, i.e. $I(t) = 0$, $N_C(t) = 0$, $\Omega_M = \Omega$ and $\tau = \infty$. As the filament grows, precise knowledge of the trajectories of molecules close to the bulk become obsolete. We replace the space behind the filament with compartments, i.e. we will describe G-actin in Ω_C in terms of $N_C(t)$ numbers $A_i(t)$, $i = 1, 2, \ldots, N_C(t)$, where $A_i(t)$ describes the number of G-actin molecules in the ith compartment at time t. When the distance from the filament tip $X(t)$ to the TRM interface $I(t)$ (or initially the bulk) reaches a critical value, a new compartment is created at the interface by counting the copy number of

Table 4 Pseudocode of one iteration of the TRM model of actin dynamics in a filopodium

[C1]	Compute the time when the next diffusive jump (19) occurs as $t_C + \tau$, where t_C is the current time in Ω_C and the time step τ is computed by (20)
[C2]	If $t_C + \tau \leq t_M + \Delta t$, then use a uniformly distributed random number to compute which diffusive jump (19) occurs at time $t_C + \tau$. Update the numbers of G-actin molecules in the corresponding compartments. If the selected jump is a "jump into Ω_M," then reduce A_{N_C} by 1, but wait to initialize this molecule in the molecular regime Ω_M until the next molecular-based time step. Go to step [C1] where the current time in Ω_C is updated to $t_C + \tau$
[C3]	If $t_C + \tau > t_M + \Delta t$, then perform steps [B1]–[B4] and [B6]–[B8] on all molecules in Ω_M. It should be noted that $y_i(t)$ and $y_i(t + \Delta t)$ in steps [B3] and [B4] are replaced by $y_i(t_M) - I(t_M)$ and $y_i(t_M + \Delta t) - I(t_M)$, where $I(t_M)$ is the current position of the inter-regime interface. If $N_C \geq 1$, then the molecules which leave Ω_M in steps [B3] and [B4] are not removed from the system but rather placed in the compartment that is at this interface, i.e., they increase A_{N_C}
[C4]	If $N_C \geq 1$, then the molecules that require initiation into the molecular-based regime are initiated a distance x from the interface $I(t_M)$ according to the distribution (11)
[C5]	If $N_C = 0$, then the step [B5] is performed
[C6]	If the distance between the filament tip and the interface $X(t_M + \Delta t) - I(t_M)$ reaches a critical value (we take this critical value to be $8h$), then $I(t_M + \Delta t) = I(t_M) + h$, $N_C(t_M + \Delta t) = N_C(t_M) + 1$ and $A_{N_C(t_M+\Delta t)}$ is given by (18)
[C7]	If the step [C6] resulted in a shift of the interface, or the step [C3] resulted in a change in A_{N_C}, then update τ by (22)
[C8]	Continue with the step [C2] where t_M is updated to $t_M + \Delta t$

G-actin inside the region of distance h from the interface and considering this to be the new compartment. In the step [C6], the movement of the interface is implemented using the molecular-based time steps (17), i.e. the TRM interface is shifted by $I(t_M + \Delta t) = I(t_M) + h$, N_C is increased by 1 and the copy number of G-actin molecules in the new final compartment that is created is equal to a count of G-actin in the molecular-based region which has just been engulfed by the interface

$$A_{N_C(t_M+\Delta t)} = \left|\left\{i \,|\, y_i(t) \in \left[I(t_M), I(t_M + \Delta t)\right]\right\}\right|. \tag{18}$$

We take the critical distance between $I(t)$ and $X(t)$ in the step [C6] to be $8h$ since we found this to be an appropriate length such that the filament tip does not retract back over this interface over the course of the simulation.

We simulate the compartment-based region Ω_C identically to that in Sect. 2.1. However, there is just diffusive jumping in this region since it does not cover the filament tip, i.e., the model of G-actin in Ω_C reads as follows:

$$\emptyset \underset{d}{\overset{d\overline{A}}{\rightleftarrows}} A_1 \underset{d}{\overset{d}{\rightleftarrows}} A_2 \underset{d}{\overset{d}{\rightleftarrows}} A_3 \underset{d}{\overset{d}{\rightleftarrows}} \cdots \underset{d}{\overset{d}{\rightleftarrows}} A_{N_C} \xrightarrow{\overline{\Phi}} \text{“jump to } \Omega_M\text{”}, \tag{19}$$

where $d = D/h^2$, $\Phi = \overline{\Phi} A_{N_C}$, and Φ is given by (14). This is implemented in the steps [C1] and [C2]. Using a uniformly distributed random number $r \in (0, 1)$, we can compute time to the next diffusive event by (3). Since the current time in Ω_C is t_C, formula (3) can be rewritten as

$$\tau = \frac{1}{\alpha_0(t_C)} \log\left(\frac{1}{r}\right), \tag{20}$$

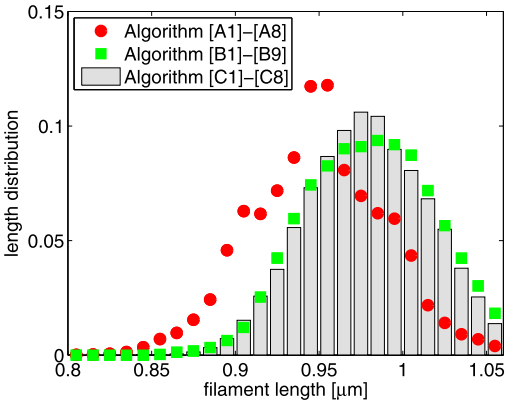

Fig. 6 Distribution of the filament length X computed by the algorithms [A1]–[A8] (*red circles*), [B1]–[B9] (*green squares*), and [C1]–[C8] (*gray histogram*). Parameters are given in Table 2

where the total propensity function corresponding to (19) is given by

$$\alpha_0(t_C) = d\overline{A} + dA_{N_C}(t_C) + \Phi(t_C) + 2d\sum_{i=1}^{N_C-1} A_i(t_C), \tag{21}$$

where $\Phi \equiv \Phi(t_C)$ is given by (14). If a diffusion jump occurs before $t_M + \Delta t$, then the step [C2] is performed. Simulation of the off-lattice region and polymerization-depolymerization kinetics is done in a similar way to Sect. 3 in the step [C3]. This step will be performed if a molecular-based time step occurs before the next compartment-based event. Here, time t is replaced by t_M. For example, the formula (8) is modified to

$$y_i(t_M + \Delta t) = y_i(t_M) + \sqrt{2D\Delta t}\xi_i,$$

i.e., the positions of molecules in Ω_M are updated at multiples of Δt given by (17) in the step [C3]. The interface between Ω_M and Ω_C is modeled using the TRM (Flegg et al. 2012) in the steps [C2]–[C4] except for the initial growth stage (step [C5]) of the model where there are no compartments in the filopodia, in which case, the boundary condition with the bulk that is described in Sect. 3 is used for consistency.

If the step [C6] results in a shift of the interface, or the step [C3] results in a change in A_{N_C}, then the propensity function (21) will change and the time step τ in the compartment-based part Ω_C will have to be updated in the step [C7] by

$$\tau := \frac{\tau\alpha_0^{\text{old}}}{\alpha_0^{\text{new}}} + (t_M + \Delta t - t_C)\left(1 - \frac{\alpha_0^{\text{old}}}{\alpha_0^{\text{new}}}\right), \tag{22}$$

where α_0^{old} and α_0^{new} are the total propensity functions computed using (21) before the most recent [C3] step and after the most recent [C6] step, respectively (Gibson and Bruck 2000; Flegg et al. 2012).

4.1 Illustrative Computational Results

Using the same parameters that were used in the previous sections, we present the results computed by the TRM algorithm [C1]–[C8] in Fig. 6. We compare them with the

Table 5 Breakdown of the computational time required for 10^3 s of simulation using the TRM algorithm [C1]–[C8] from Sect. 4 and the molecular-based model [B1]–[B9] from Sect. 3. The parameters that were used in these simulations can be found in Table 2

Computational process	TRM algorithm [C1]–[C8] (hrs)	Molecular-based model [B1]–[B9] (hrs)	Saving (%)
Flux to/from bulk	1.79	2.68	33
Diffusion in Ω_M	2.77	2.76	0
Diffusion in Ω_C	0.06	2.36	97
Filament tip kinetics/polymerization	4.21	4.27	1
Other	0.12	0.12	0

results computed by the minimal hybrid model [A1]–[A8] and the molecular-based algorithm [B1]–[B9]. Since molecules inside the compartments need to be updated rarely (only when they jump from compartment to compartment) significant savings in computational effort can be made while still achieving the same accuracy as the molecular-based model [B1]–[B9].

Our illustrative simulations were implemented in Matlab R2012a using an AMD Athlon 64 X2 dual core processor 5200+. To run the molecular-based algorithm [B1]–[B9] until a maximum time of 10^3 s, just over 12 hours of simulation time was required. On the same computer, the TRM simulation (algorithm [C1]–[C8]) took just under 9 hours for a saving of around 25 %. This number will be larger or smaller depending on the simulation parameters. To explain where the computational savings come from, we present a more detailed breakdown of the computational effort in Table 5. We present times spent in different subroutines of the computer implementations of algorithms [C1]–[C8] and [B1]–[B9].

It is not surprising that a large portion of observed computational saving was from diffusion of G-actin outside of the region of interest. G-actin jumps from compartment to compartment are rare in the TRM each timestep Δt, whereas G-actin that is modeled using a molecular-based approach [B1]–[B9] requires constant updating. The time spent simulating the diffusion of molecules in the region of interest Ω_M, however, did not change because the same numerical technique was used for these molecules in both algorithms. There was no saving in time required to polymerize and depolymerize at the filament tip since this is done using the same molecular-based technique in both simulations, and as already discussed, this is unavoidable if high accuracy is demanded of the simulation. A small saving was made at the interface of the filopodia with the bulk since this interface in the TRM model is a compartment boundary which is simpler to implement. For reaction–diffusion processes which involve heavy computational effort in large regions that are of less significant biological interest, the TRM potentially could reduce the simulation of such processes by large amounts while still retaining the accuracy of the simulation where it is needed (Flegg et al. 2012). For example, in longer filopodia, which can grow to 3–4 μm (Zhuravlev and Papoian 2009) the time savings of the TRM method could be significantly larger than 25 % (because a larger portion of filopodia would be treated via a compartment based model).

5 Discussion

In this paper, we have presented three different approaches to stochastic reaction–diffusion simulations for a simple model of actin filament dynamics in filopodia. In the first approach, we consider a hybrid modeling technique which was used in the literature (Zhuravlev and Papoian 2009; Zhuravlev et al. 2010). We developed the minimal hybrid model [A1]–[A8], which contains main features of the actin dynamics. The polymerization at the barbed end grows the filament while depolymerization and retrograde flow act to reduce the length of the filament until a steady state is reached. G-actin is allowed to diffuse in a discretize domain by means of a random walk from compartment to compartment. Polymerization may occur when the tip of the filament is inside the same compartment as the reacting G-actin. This model is less computationally intensive than other presented approaches.

The second model [B1]–[B9] is a more detailed off-lattice molecular-based model whereby each G-actin monomer diffuses in continuous space by means of Gaussian distributed displacements at each time step. The advantage of this approach is that one can use a more complex description of polymerization and depolymerization events. Since we wanted a "fair comparison" between algorithms [A1]–[A8] and [B1]–[B9], we used relatively straightforward implementation of the biochemistry at the barbed end of the actin filament. However, the model [B1]–[B9] could be further enhanced by considering a suitable reaction radius (Lipkova et al. 2011) or binding and unbinding radii (Andrews and Bray 2004; Andrews 2005) corresponding to actin polymerization and depolymerization events. This is the main strength of the molecular-based approaches of the form [B1]–[B9]. Their disadvantage is that they are often more computationally intensive. This is because, the accuracy of the simulation is derived from the precision of the distribution of monomers and, therefore, their potential to polymerize. The cost of this knowledge is that these molecules are tracked throughout the whole domain regardless of their likelihood to polymerize (that is, regardless of their proximity to the filament tip). This tracking of every single molecule in continuous space can lead to larger computational times.

The third approach that is presented in this paper utilizes a molecular-based model in the region around the filament tip, but models monomers that are not in the proximity of the tip as random walkers on a lattice so that significant computational time may be spared. The coupling of the on- and off-lattice regions is done using the TRM (Flegg et al. 2012). It was shown that the model results were similar to a fully molecular-based model but computational time could be improved by not tracking all particles in continuous space at each time step.

For stochastic reaction–diffusion models whereby a particular region of interest exists that drives the system, each of the presented methods may be used. Compartment-based models are quick and simple but this is at the cost of losing some accuracy in the simulated results, which may become problematic especially in the presence of steep spatial gradients of the cytosolic chemicals. Confidence can be given to molecular-based models if the time step is small enough. The TRM may offer a compromise between performance and accuracy by carefully choosing regions in which higher precision in the model is necessary. However, if one needs to simulate very large actin networks, such as micron-size three-dimensional patches of a

lamellipodium (Hu and Papoian 2010), the computational efficiency of the less accurate compartment based algorithms may remain indispensable at least in the near future.

In Sect. 4, we presented only one possible way to make use of the TRM (Flegg et al. 2012). Another application would be to improve the modeling of coupling of filopodia with the bulk as it is schematically shown in Fig. 5(b). In Sect. 3, the boundary condition at the bulk assumes that there is a compartment outside the off-lattice domain in the bulk that has the expected number of molecules $\overline{A}$. Of course, in reality the number of molecules in this compartment would necessarily fluctuate, therefore, it would be possible to model the bulk using the TRM over a region that penetrates into the bulk (Flegg et al. 2013). We did not introduce this complication because we wanted to model the bulk boundary in the same way as in the minimal hybrid model [A1]–[A8] to enable easier comparison of different modeling approaches. We focused on the case of moving interface $I(t)$, which is itself a generalization of the TRM and can be nontrivial in more complicated situations (Ho 2012). Another possible way to accelerate simulation would be to couple molecular-based or compartment-based models with macroscopic partial differential equations in the bulk or near the bulk end of a filopodium (Wagner and Flekkøy 2004; Moro 2004; Franz et al. 2013; Ferm et al. 2010; Flekkøy et al. 2001).

Acknowledgements The research leading to these results has received funding from the European Research Council under the *European Community*'s Seventh Framework Programme (*FP7/2007–2013)*/ ERC *grant agreement* No. 239870. Radek Erban would also like to thank Brasenose College, University of Oxford, for a Nicholas Kurti Junior Fellowship; the Royal Society for a University Research Fellowship; and the Leverhulme Trust for a Philip Leverhulme Prize. This prize money was used to support a research visit of Garegin Papoian in Oxford. Garegin Papoian was also supported by the National Science Foundation CAREER Award CHE-0846701.

References

Andrews, S. (2005). Serial rebinding of ligands to clustered receptors as exemplified by bacterial chemotaxis. *Phys. Biol.*, *2*, 111–122.

Andrews, S., & Bray, D. (2004). Stochastic simulation of chemical reactions with spatial resolution and single molecule detail. *Phys. Biol.*, *1*, 137–151.

Arjunan, S., & Tomita, M. (2010). A new multicompartmental reaction–diffusion modeling method links transient membrane attachment of E. coli MinE to E-ring formation. *Syst. Synth. Biol.*, *4*(1), 35–53.

Cao, Y., Li, H., & Petzold, L. (2004). Efficient formulation of the stochastic simulation algorithm for chemically reacting systems. *J. Chem. Phys.*, *121*(9), 4059–4067.

Engblom, S., Ferm, L., Hellander, A., & Lötstedt, P. (2009). Simulation of stochastic reaction–diffusion processes on unstructured meshes. *SIAM J. Sci. Comput.*, *31*, 1774–1797.

Erban, R., & Chapman, S. J. (2007). Reactive boundary conditions for stochastic simulations of reaction–diffusion processes. *Phys. Biol.*, *4*(1), 16–28.

Erban, R., & Chapman, S. J. (2009). Stochastic modeling of reaction–diffusion processes: algorithms for bimolecular reactions. *Phys. Biol.*, *6*(4), 046001.

Erban, R., Chapman, S. J., & Maini, P. (2007). *A practical guide to stochastic simulations of reaction–diffusion processes*, 35 pages, arXiv:0704.1908.

Ferm, L., Hellander, A., & Lötstedt, P. (2010). An adaptive algorithm for simulation of stochastic reaction–diffusion processes. *J. Comput. Phys.*, *229*, 343–360.

Flegg, M., Chapman, J., & Erban, R. (2012). The two-regime method for optimizing stochastic reaction–diffusion simulations. *J. R. Soc. Interface*, *9*(70), 859–868.

Flegg, M., Rüdiger, S., & Erban, R. (2013). Diffusive spatio-temporal noise in a first-passage time model for intracellular calcium release. *J. Chem. Phys.* doi:10.1063/1.4796417.

Flekkøy, E., Feder, J., & Wagner, G. (2001). Coupling particles and fields in a diffusive hybrid model. *Phys. Rev. E*, *64*, 066302.

Franz, B., Flegg, M., Chapman, J., & Erban, R. (2013, to appear). Multiscale reaction–diffusion algorithms: PDE-assisted Brownian dynamics. *SIAM J. Appl. Math.* arXiv:1206.5860.

Gibson, M., & Bruck, J. (2000). Efficient exact stochastic simulation of chemical systems with many species and many channels. *J. Phys. Chem. A*, *104*, 1876–1889.

Gillespie, D. (1977). Exact stochastic simulation of coupled chemical reactions. *J. Phys. Chem.*, *81*(25), 2340–2361.

Hattne, J., Fange, D., & Elf, J. (2005). Stochastic reaction–diffusion simulation with MesoRD. *Bioinformatics*, *21*(12), 2923–2924.

Hepburn, I., Chen, W., Wils, S., & De Schutter, E. (2012). STEPS: efficient simulation of stochastic reaction–diffusion models in realistic morphologies. *BMC Syst. Biol.*, *6*, 36.

Ho, C.-P. (2012). *Multi-scale reaction diffusion simulations in biology*. M.Sc. Thesis, University of Oxford.

Hu, L., & Papoian, G. A. (2010). Mechano-chemical feedbacks regulate actin mesh growth in lamellipodial protrusions. *Biophys. J.*, *98*(8), 1375–1384.

Lan, Y., & Papoian, G. A. (2008). The stochastic dynamics of filopodial growth. *Biophys. J.*, *94*, 3839–3852.

Lipkova, J., Zygalakis, K., Chapman, J., & Erban, R. (2011). Analysis of Brownian dynamics simulations of reversible bimolecular reactions. *SIAM J. Appl. Math.*, *71*(3), 714–730.

Moro, E. (2004). Hybrid method for simulating front propagation in reaction–diffusion systems. *Phys. Rev. E*, *69*, 060101.

Noselli, S. (2002). Drosophila, actin and videotape—new insights in wound healing. *Nat. Cell Biol.*, *4*, 251–253.

Opplestrup, T., Bulatov, V., Donev, A., Kalos, M., Gilmer, G., & Sadigh, B. (2009). First-passage kinetic Monte Carlo method. *Phys. Rev. E*, *80*(6), 066701.

Schaus, T., Taylor, E., & Borisy, G. (2007). Self-organization of actin filament orientation in the dendritic-nucleation/array-treadmilling model. *Proc. Natl. Acad. Sci. USA*, *104*, 7086–7091.

Stiles, J., & Bartol, T. (2001). Monte Carlo methods for simulating realistic synaptic microphysiology using MCell. In E. Schutter (Ed.), *Computational neuroscience: realistic modeling for experimentalists* (pp. 87–127). Boca Raton: CRC Press.

van Zon, J., & ten Wolde, P. (2005). Green's-function reaction dynamics: a particle-based approach for simulating biochemical networks in time and space. *J. Chem. Phys.*, *123*, 234910.

Wagner, G., & Flekkøy, E. (2004). Hybrid computations with flux exchange. *Philos. Trans. R. Soc. A, Math. Phys. Eng. Sci.*, *362*, 1655–1665.

Yamazaki, D., Kurisu, S., & Takenawa, T. (2005). Regulation of cancer cell motility through actin reorganization. *Cancer Sci.*, *96*(7), 379–386.

Zhuravlev, P., & Papoian, G. (2009). Molecular noise of capping protein binding induces macroscopic instability in filopodial dynamics. *Proc. Natl. Acad. Sci. USA*, *106*(28), 11570–11575.

Zhuravlev, P., & Papoian, G. A. (2011). Protein fluxes along the filopodium as a framework for understanding the growth-retraction dynamics: the interplay between diffusion and active transport. *Cell Adhes. Migr.*, *5*(5), 448–456.

Zhuravlev, P., Der, B., & Papoian, G. A. (2010). Design of active transport must be highly intricate: a possible role of myosin and ena/VASP for G-actin transport in filopodia. *Biophys. J.*, *98*, 1439–1448.

Zhuravlev, P., Lan, Y., Minakova, M., & Papoian, G. A. (2012). Theory of active transport in filopodia and stereocilia. *Proc. Natl. Acad. Sci. USA*, *109*, 10849–10854.